Atmospheric Environment 324 (2024) 120417

Contents lists available at ScienceDirect

Atmospheric Environment

journal homepage: www.elsevier.com/locate/atmosenv

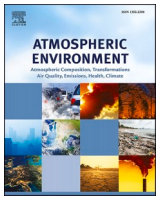

Exploring ozone production sensitivity to NO_x and VOCs in the New York City airshed in the spring and summers of 2017–2019

Abby E. Sebol [a,*], Timothy P. Canty [a], Glenn M. Wolfe [b], Reem Hannun [b,c], Allison M. Ring [a], Xinrong Ren [a,d]

[a] Department of Atmospheric and Oceanic Science, University of Maryland, College Park, United States
[b] Atmospheric Chemistry and Dynamics Laboratory, NASA Goddard Space Flight Center, United States
[c] Department of Geology and Environmental Science, University of Pittsburgh, United States
[d] Air Resources Laboratory, National Oceanic and Atmospheric Administration, United States

HIGHLIGHTS

- Ozone production is faster in the morning than in the afternoon.
- VOC-limited ozone production is frequent along the Connecticut coastline and in NYC.
- Ozone production sensitivity to biogenic and anthropogenic VOC varies with season and time of day.
- Greater ozone production is calculated using MCMv3.3.1 compared to CB6r2, though both exhibit similar NO_x sensitivity.

ARTICLE INFO

Keywords:
Air quality
Long Island Sound Tropospheric Ozone Study (LISTOS)
Framework for 0-D atmospheric modeling (F0AM)
Ozone production
NO_x
VOCs

ABSTRACT

Reducing ozone in the New York City (NYC) region requires understanding the nonlinearity of ozone production (PO_3) and its sensitivity to volatile organic compounds (VOCs) and nitrogen oxides ($NO_x = NO_2 + NO$). Using observations from the Long Island Sound Tropospheric Ozone Study (LISTOS) in the late spring and summers of 2017–2019 and a 0-D box model, we test the sensitivity of PO_3 to ozone precursors. PO_3 is greater in the morning than the afternoon due to increased concentrations of NO_2 and VOC. This diurnal variation in PO_3 is enhanced in the late summer. Based on the model response of PO_3 to changes in initial NO_2, 14% of samples are within a VOC-limited regime. The metric LRO_x/LNO_x, which compares the radical loss rates via self-reaction to their reaction with NO_2, indicates an additional 17% of samples are in transition between NO_x and VOC-limited regimes ($0.30 <= LRO_x/LNO_x <= 1$). We often find PO_3 to be VOC-limited in NYC and along the Connecticut coastline (I-95 corridor). In these samples, PO_3 is most sensitive to isoprene, propene, and isopentane, and individual VOCs have strong diurnal and seasonal variations. We further compare PO_3 calculations using the near explicit Master Chemical Mechanism (MCMv3.3.1) and Carbon Bond 6 revision 2 (CB6r2) for a more direct link to regulatory air quality models. Modeled PO_3 is 20% greater in MCMv3.3.1, due largely to the speciation of VOC and organic peroxy radicals, however the bounds of LRO_x/LNO_x used to determine the transition range between PO_3 regimes remain the same.

1. Introduction

Surface ozone is responsible for one million premature deaths globally every year (Anenberg et al., 2010; Malley et al., 2017). Despite significant reductions in ozone precursors in recent decades, an estimated 120 million people live in areas that surpass the EPA's national air quality standard for ozone of 70 ppb over an 8-h average. There are 20 million people in the New York (NY)-New Jersey (NJ) -Connecticut (CT) region which is classified by the EPA as 'moderately' out of attainment (EPA, 2023).

Abbreviations: LISTOS, Long Island Sound Tropospheric Ozone Study; PO_3, ozone production; VOC, Volatile Organic Compound; F0AM, Framework for 0-D Atmospheric Modeling; MCM, Master Chemical Mechanism version 3.3.1; CB6r2, Carbon Bond mechanism version 6 revision 2.

* Corresponding author. 4254 Stadium Dr, College Park, MD, 20742, United States.
E-mail address: asebol@umd.edu (A.E. Sebol).

https://doi.org/10.1016/j.atmosenv.2024.120417
Received 20 October 2023; Received in revised form 18 January 2024; Accepted 19 February 2024
Available online 20 February 2024

Ozone production (PO_3) in the troposphere is driven by the oxidation of carbon monoxide (CO) and volatile organic compounds (VOCs) in the presence of nitrogen oxides ($NO_2 + NO = NO_x$). PO_3 is nonlinear with respect to precursor concentrations due to the relative importance of radical termination reactions. In relatively low NO_x environments (NO_x-limited regime), radical self-reaction is the predominant termination step:

$$HO_2 + HO_2 \rightarrow H_2O_2 + O_2 \quad (R1)$$

$$HO_2 + RO_2 \rightarrow ROOH + O_2 \quad (R2)$$

$$RO_2 + RO_2 \rightarrow ROOR + O_2 \quad (R3)$$

Under these conditions, lowering NO_x concentrations will decrease PO_3. In relatively high NO_x environments (VOC-limited regime), the formation of nitric acid is the main terminating reaction:

$$NO_2 + OH + M \rightarrow HNO_3 + M \quad (R4)$$

Under this regime, lowering NO_x concentrations will increase PO_3. The transition between regimes occurs when NO_x decreases to the point where the rates of R1-R3 become greater than R4.

Several metrics are available to classify the PO_3 regime. The Empirical Kinetic Modeling Approach (EKMA) utilizes a 0-dimensional box model constrained by observations or estimated emissions of NO_x and VOCs. Varying input concentrations or emissions in the model tests the sensitivity of PO_3 to effectively map the NO_x and VOC space.

Another method involves comparing radical loss rates of self-reaction (LRO_x, sum of reactions R1-R3) to the reaction with NO_2 (LNO_x, reaction R4). If ozone production was only determined by radical destruction, the transition point would be where $LRO_x/LNO_x = 1$. However, past studies have highlighted a discrepancy between these techniques. The value of NO_x where $LRO_x/LNO_x = 1$ is less than the value of NO_x at the peak PO_3 transition point determined by the EKMA isopleths. At the transition point on the EKMA curves, LRO_x/LNO_x is estimated to be 0.37 by Kleinman et al. (2001); Schroeder et al. (2017) estimates this threshold to be 0.25–0.45 with a median of 0.35, based on observations from several U.S. urban areas.

Effective NO_x controls have transitioned much of the NYC region to a NO_x-limited regime (He et al., 2020; Roberts et al., 2022). Complex and changing emission sources, however, challenge efforts to quantify spatial and temporal variations of PO_3 in this region (Chen et al., 2019). Anthropogenic emissions of NO_x and VOCs are transported into the region via prevailing westerly winds (long range transport) or emitted directly from NYC (local emissions) and transported downwind. Local sources include industrial and manufacturing activity, energy production, traffic and volatile chemical products (personal care products, pesticides, paints, etc.) (Coggon et al., 2021; Gkatzelis et al., 2021; McDonald et al., 2018; Oliveira et al., 2023). Biogenic VOCs (BVOC) also contribute to total atmospheric loadings in NYC from forested regions (Chen et al., 2019). Season and time of day affect the relative impact of BVOC (Ring et al., 2023).

We use airborne observations of reactive gases acquired in and around NYC in the spring and summers of 2017–2019 to derive spatial and temporal patterns in ozone production. We constrain a box model with these observations to test the sensitivity of PO_3 to changes in initial concentrations of NO_x and individual VOCs. We compare this sensitivity between morning and afternoon samples as well as seasonal differences. With these results, we investigate the transition point between NO_x and VOC-limited air samples using the slope of the PO_3 curve and LRO_x/LNO_x. We estimate PO_3 using both nearly explicit and lumped mechanisms to investigate the differences in their respective RO_2 and PO_3 representation. This comparison puts our results into context with regulatory air quality modeling which utilizes lumped mechanisms.

2. Methods

2.1. Aircraft observations

This study analyzes aircraft data from two flight campaigns. The Long Island Sound Tropospheric Ozone Study (LISTOS: https://www-air.larc.nasa.gov/missions/listos/) was a multi-agency project to investigate air quality within the NY metropolitan area during July and August 2018 and 2019. The Regional Atmospheric Measurement Modeling and Prediction Program (RAMMPP), led by the University of Maryland, is a long-term effort to study air quality in the Eastern United States through both in situ observations and large-scale chemical modeling. We use RAMMPP data collected in May 2017 within the same study domain as LISTOS (Fig. 1).

Flights utilized a CESSNA 402B aircraft equipped with in situ measurements of ozone, NO, NO_2, CO, SO_2, CH_4, CO_2, and meteorological parameters, including ambient temperature, relative humidity, pressure, wind speed and direction. A complete description of the aircraft instrumentation can be found in Ren et al. (2018). Some flights in 2018 and 2019 also included observations of formaldehyde (HCHO) from the NASA Compact Airborne Formaldehyde Experiment (CAFE) (St Clair et al., 2019).

The whole air samples collected in canisters were analyzed for VOC concentrations offline with Gas Chromatography- Flame Ionization Detection or Mass Spectrometry. Table S1 lists all reported VOCs. All continuously monitored state variables and chemical species were averaged over the whole air sampling window, typically spanning about 2 min.

A total of 118 samples were taken from 2017 to 2019 over the Long Island Sound (LIS) region; here we only consider the 107 samples that were accompanied by valid NO_2 observations and within the domain of interest (Fig. 1). Of these, 34 were collected in the morning (before 12:00 EDT) and 73 in the afternoon (after 12:00 EDT). All were collected at altitudes of 1.5 km or less. Simultaneous HCHO observations are available for 41 of 107 samples.

2.2. Box model

We use the Framework for 0-D Atmospheric Modeling (F0AM) version 3 (Wolfe et al., 2016) to model PO_3. Simulations are constrained to observations of temperature, pressure, relative humidity, CH_4, NO_2,

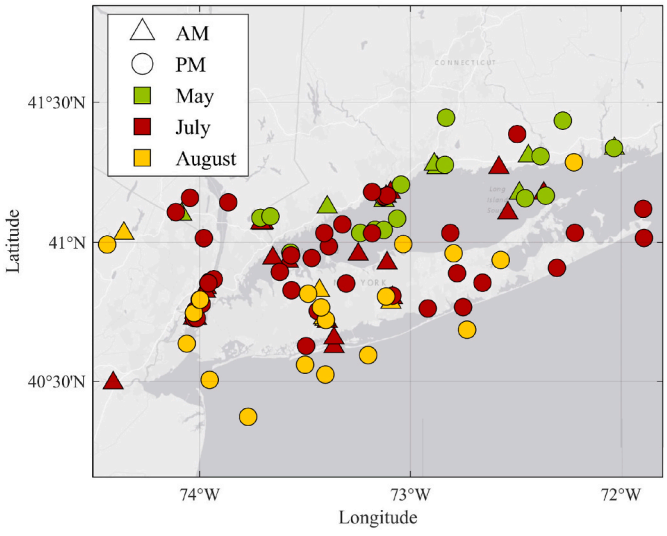

Fig. 1. Location of the LISTOS whole air samples. Triangle markers indicate morning observations (before local noon), circles for the afternoon observations (after local noon). Green, red, and yellow are observations taken in May, July, and August, respectively. All observations are taken below 1.5 km.

NO, O_3, SO_2, and all measured VOCs except HCHO. Unobserved species are initialized at 0 ppb. HCHO observations are used for sensitivity tests as described in Supplemental Text S1and are not included in the box model as they are not available for all samples.

Photolysis frequencies are estimated using F0AM's "hybrid" parameterization, which combines solar spectra from the Tropospheric Ultraviolet and Visible Radiation Model (TUV) with quantum yields and cross sections from the IUPAC (Atkinson et al., 2004, 2006) and JPL (Sander et al., 2011) databases. Given inputs of solar zenith angle (SZA), altitude, overhead ozone, and surface albedo, look up tables provide previously calculated photolysis frequencies (j values). We assume clear sky conditions and constant overhead ozone (325 DU) and surface albedo (0.2).

We utilize both the Master Chemical Mechanism version 3.3.1 (hereafter referred to as MCM; Jenkin et al., 2015) and Carbon Bond 6 version 2 (CB6r2; Hildebrandt Ruiz and Yarwood, 2013) chemical mechanisms. We implement a subset of the full MCM including 13,424 reactions and 4475 species, tailored to available observations. CB6r2 contains 216 reactions and 77 explicit species or families of species. Rate constants for reactions involving the families in CB6r2 are often based on the rate of a single, representative species (Gery et al., 1989). We include CB6r2 for contrast with the explicit MCM and to more directly link the results to regulatory air quality models. Unless otherwise stated, results represent output from MCM-based simulations. Some measured VOCs are not included in either chemical mechanism (Table S1).

For each set of observations, we run F0AM for 24 h at 15-min time steps with photolysis frequencies evolving along the diurnal cycle. We initialize and hold all observed species constant. Total NO_x is held constant while NO and NO_2 are allowed to partition internally. A physical loss lifetime of 24 h is applied to all species to prevent build-up of long-lived species. One day of model simulations may not be sufficient to reach full steady state in all cases, but model results and our conclusions do not change significantly for longer integration times. To test this, we extended the integration time to the point when OH, HO_2, and HCHO reached convergence, defined as a day-to-day change of less than 0.1%. On average, this took four days of integration time and reduced PO_3 by 6%.

This simulation framework is consistent with prior box model studies of PO_3 and VOC chemistry (Crawford et al., 1999; Lindsay et al., 2022; Marvin et al., 2017; Mazzuca et al., 2016; Olson et al., 2001, 2004; Schroeder et al., 2016, 2017; Souri et al., 2020). Instantaneous PO_3 is calculated at the end point of each model run.

$$PO_3 = k_{NO,HO2}[NO][HO_2] + \sum(k_i[NO][RO_2]_i) - (k_{OH,O3}[OH][O_3] + k_{HO2,O3}[O_3][HO_2] + k_{NO2,OH}[NO_2][OH] + \sum(k_i[O_3][VOC]_i) + j[O_3]) \quad (5)$$

where the first two terms are production terms and the last 5 are loss terms. We calculate LRO_x/LNO_x using reactions R1- R4. OH reactivity (OHr) is defined as

$$OHr = \sum k_{i,OH}[VOC]_i \quad (6)$$

where $k_{i,OH}$ is the rate constant for the reaction between hydroxyl (OH) and each individual VOC and $[VOC]_i$ is the corresponding concentration.

Several sensitivity tests probe the response of PO_3 to NO_x and VOCs. To generate traditional PO_3 curves as a function of NO_x, we modify initial NO_2 from 0.01 to 30 ppb while holding VOCs constant. Separately, we test local VOC sensitivity by changing the initial concentrations of VOCs by ±1% while holding NO_x constant.

3. Results and discussion

3.1. PO_3 sensitivity to NO_x

3.1.1. Transition region

Fig. 2 shows 107 PO_3 curves individually generated from each sample by varying initial NO_2. Median PO_3 is represented as the bold blue line. On average, peak PO_3 is 23 ppb/h and occurs at a NO_2 mixing ratio of 5.1 ppb. Median observed NO_2 (black circle) is 1.8 ppb and corresponds to median PO_3 of 13 ppb/h. This value of PO_3 corresponding to observed NO_2 is hereafter referred to as 'control PO_3'.

Based on $d[PO_3]/d[NO_2]$ (henceforth referred to as the 'slope') at each observed NO_2 point, 92 samples (86%) are within NO_x-limited regime and 15 samples (14%) are within VOC-limited regime, where NO_x-limited is defined as a positive slope and VOC-limited is defined as a negative slope. There is a difference in the control PO_3 between regimes; NO_x-limited regimes have a median of 14.5 ppb/h at the observed NO_2 and VOC-limited regimes have a median of 20.5 ppb/h.

We use LRO_x/LNO_x to investigate the magnitude of the PO_3 response to changes in both VOCs and NO_x. At the peak of the PO_3 curves, LRO_x/LNO_x ranges from 0.15 to 0.54 (Fig. S1) and has an average value of 0.30 (pink triangle). Schroeder et al. (2017) provides a range of 0.25–0.45 for LRO_x/LNO_x at peak PO_3 using data over several years and multiple urban cities in the United States. Different VOC observations are likely responsible for the variation in average peak value. Despite the diverse environments, the value of LRO_x/LNO_x at the peak PO_3, does not drastically change.

LRO_x/LNO_x is equal to one (yellow square) at NO_x values below the peak of the PO_3 curve. This is the point at which the radical removal rates via peroxide and nitric acid formation are equal. The relationship between slope and LRO_x/LNO_x is illustrated further in Fig. S2. We define the range $0.3<=LRO_x/LNO_x<=1$ as the "transition region" between NO_x and VOC-limited regimes. In this transition region, reductions in NO_x and VOC both reduce PO_3, but VOCs have a greater impact per molecule. In a sense, PO_3 is neither NO_x nor VOC-limited in this range. Using this definition, 17 observations (16%) are in transition. This method of defining transition emphasizes the importance of VOCs along with NO_x in lowering ozone production and provides greater detail in defining the shift between NO_x and VOC-limited regimes.

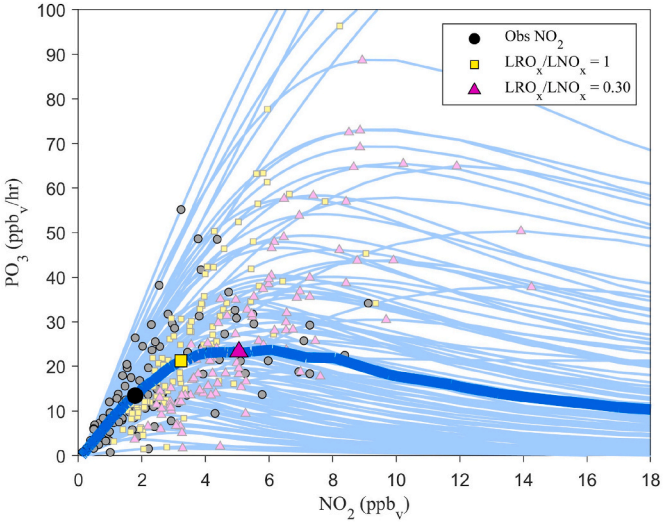

Fig. 2. Individual PO_3 (ppb/hr) as a function of initial NO_2 concentration (n = 107). The bold blue line represents the median PO_3 curve. Each line includes the observed NO_2 (black/gray circle), LRO_x/LNO_x = 1 (yellow square), and LRO_x/LNO_x = 0.30 (pink triangle).

3.1.2. Spatial variability of PO_3 regime

Fig. 3 maps the designated PO_3 regime as defined by LRO_x/LNO_x (Fig. S3 shows a map of the PO_3 regime as defined by the sign of the slope). As previously stated, most of the samples (73% based on LRO_x/LNO_x) are in a NOx-limited regime (red circle). This is especially true over Long Island and the Long Island Sound. However, along the Hudson River and CT coastline (I-95 corridor), we find several samples with a VOC-limited regime (blue triangle) or in transition (white square). Transportation and other industrial activities emit sufficient NO_x to sustain a VOC-limited regime. Coastal meteorology may also play a role due to the recirculation of marine air through sea breezes (Couillard et al., 2021; Loughner et al., 2014; Mazzuca et al., 2017, 2019).

3.1.3. Diurnal and seasonal variability

Past studies show that PO_3 is faster and more VOC-limited in the morning than afternoon due to a lower boundary layer in the morning which concentrates ozone precursors closer to the surface (Baier et al., 2015; Chen et al., 2010; Mao et al., 2010; Mazzuca et al., 2016; Ring et al., 2023; Strode et al., 2019). PO_3 also increases in the later summer due to greater emissions of reactive BVOC (Coates et al., 2016).

In Fig. 4, PO_3 is grouped by month and time of day (See Fig. S4 for only the AM and PM groupings). Here, the mean PO_3 curves for the entire month (blue) as well as AM (purple) and PM (orange) are included. The mean observed NO_2 values at their corresponding control PO_3 are marked as black circles.

Peak PO_3 is greater in the morning than the afternoon for all months with August having the most apparent diurnal difference. Control PO_3 is greater in the morning in the months of May and August while July has slightly higher control PO_3 in the afternoon due to greater observed NO_2 concentrations in this month. Photolysis frequency variability plays a minor role in these differences as flights typically occurred during daytime fair-weather conditions. Calculated jNO_2 and jO^1D correlate poorly with PO_3 (R^2 is 0.20 and 0.19, respectively).

The proportion of VOC-limited PO_3 samples is similar for both morning and afternoon. In the morning 5 of the samples are in a VOC-limited regime (14%) and in the afternoon 10 are in a VOC-limited regime (13%). Greater VOC concentrations in the morning shift the peak PO_3 upwards and towards higher NO_2 values. While morning NO_2 is on average greater than the afternoon, peak PO_3 is not exceeded more frequently.

May has the lowest potential for ozone production and is most likely to be in transition or in a VOC-limited regime. May exhibits the lowest peak PO_3 (17 ppb/h) and based on the average observed NO_2, most samples are near the maximum potential of PO_3. There is greater peak PO_3 in the summer months; July and August have an average peak PO_3 of 37 ppb/h and 26 ppb/h, respectively. Increased isoprene emissions in the summer boosts total OH reactivity and (given sufficient NO_2) increases potential PO_3. However, these months are not experiencing their maximum potential of PO_3 due to lower observed NO_2. The average control PO_3 is greatest in July (22 ppb/h) while May and August have similar values (15 and 12 ppb/h, respectively).

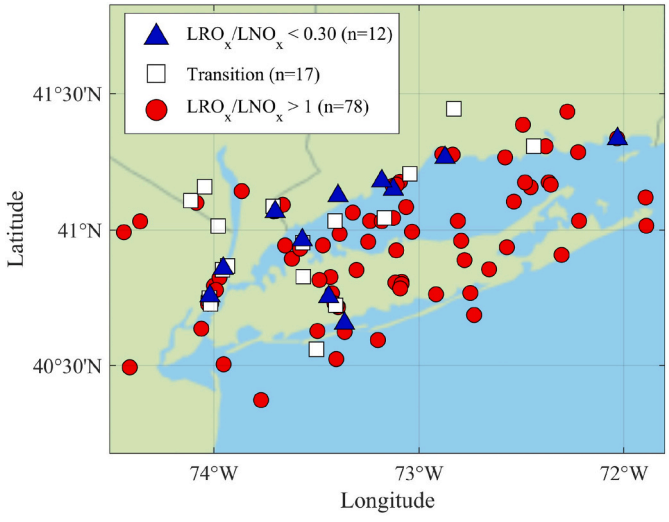

Fig. 3. Map of ozone production regime for each sample as classified by LRO_x/LNO_x at observed NO_2. Blue triangles represent a VOC-limited regime and red circles a NO_x limited regime. The LRO_x/LNO_x transition region between 0.30 and 1 is represented by white squares.

Photolysis frequencies are similar across all months implying that solar radiation does not impact the seasonal pattern of modeled PO_3 in this study. The median values of jNO_2 for May, July, and August are 0.009, 0.011, and 0.011 s^{-1}, respectively. Median values of jO^1D are 1.9 $\times 10^{-5}$, 2.8 $\times 10^{-5}$, and 2.3 $\times 10^{-5}$ s^{-1} in the same order. Note that this is only an approximation of typical clear sky conditions for these periods. Median temperatures of the aircraft observations are similar in all months, 26.6 °C, 28.2 °C, and 25.8 °C suggesting that temperature-dependent reaction rate coefficients are also not likely to be driving the seasonal variation in PO_3.

May has the largest percentage of PO_3 that is VOC-limited (27% based on slope) and in transition (19% using LRO_x/LNO_x). For these cases, lowering VOC concentrations would lead to a greater reduction, per molecule, of PO_3. On average, morning PO_3 in May is VOC-limited while the afternoon is NO_x-limited but near the transition. PO_3 in July is mostly NO_x-limited (14%), and in August is completely NO_x-limited. These months have the highest isoprene emissions and total OH reactivity. These results highlight that ozone control strategies must consider seasonally varying chemistry.

May observations were predominantly taken in the Long Island Sound and near the CT coast, while July and August samples were more concentrated over Long Island and NYC (Fig. 1). Comparison of spatial subsets for each month suggests that averages are representative of the domain even though sampling does not perfectly overlap (Text S1).

3.2. VOC sensitivity

Fig. 5 shows PO_3 sensitivity for VOCs to which modeled PO_3 is most sensitive, focusing on the 15 samples with VOC-limited PO_3. Initial VOC concentrations were altered ±1%, one species at a time and the corresponding percent change in PO_3 from the base simulations observations is calculated. Species with less than 3 valid observations in this subset are not included. Fig. 5a shows the diurnal variation of VOC sensitivity and Fig. 5b shows the seasonal variation between May and July (there were no samples within a VOC-limited regime in August). By defining PO_3 sensitivity to a percent change in initial concentrations, this metric inherently accounts for both the quantity and reactivity or each VOC. The percent change of PO_3 due to percent change of NO_2, based on the NO_2 sensitivity results (Fig. 2), is included for comparison. Because we focus on a subset with VOC-limited PO_3, the sensitivity of PO_3 to NO_2 is negative by definition.

As shown in Fig. 5, PO_3 is most sensitive to isoprene. A 1% change of isoprene causes, on average, a 0.28% change in PO_3. Isoprene comprises 7% of the total OH reactivity, the largest constituent of the measured organics, and 0.73% of total observed non-methane VOC on a per-molecule basis. The next most important VOC for PO_3 is propene which causes a 0.12% change in PO_3 per percent change in initial concentration. Propene makes up 1.9% of total OH reactivity and 0.72% of total non-methane VOC mixing ratio. While sharing a similar percentage of total concentration as propene, isoprene is a much more reactive VOC and will produce more ozone per molecule. After isoprene and propene, PO_3 is most sensitive to isopentane, toluene, and butane, all of which are anthropogenic VOC.

The chemical composition of the atmosphere varies diurnally and seasonally. The only VOC that exhibits greater PO_3 sensitivity in the afternoon than the morning is isoprene. As the day progresses, warmer

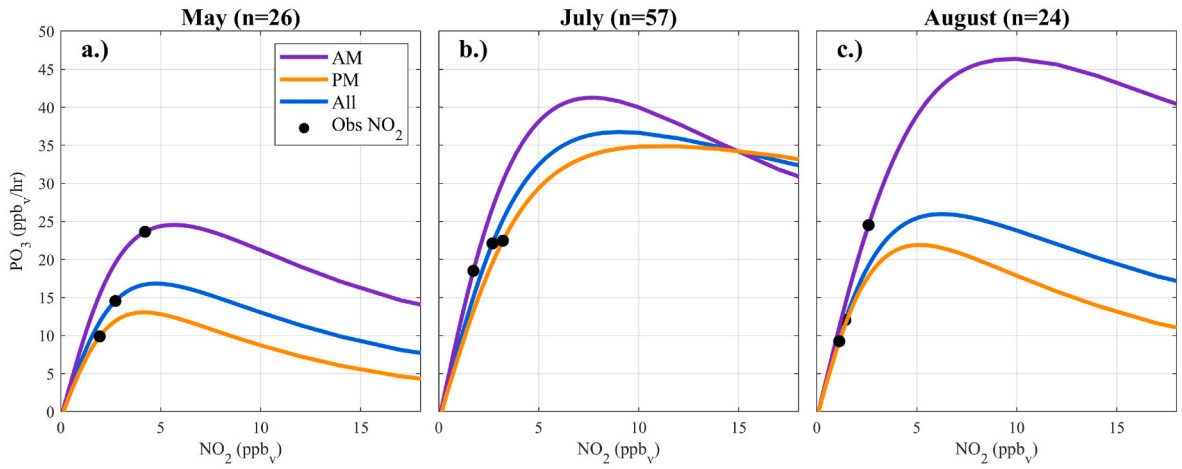

Fig. 4. Mean PO_3 in **(a)** May (n = 26), **(b)** July (n = 57), and **(c)** August (n = 24). Each month includes AM (purple), PM (orange) and all samples (blue). Observed NO_2 are indicated by black circles.

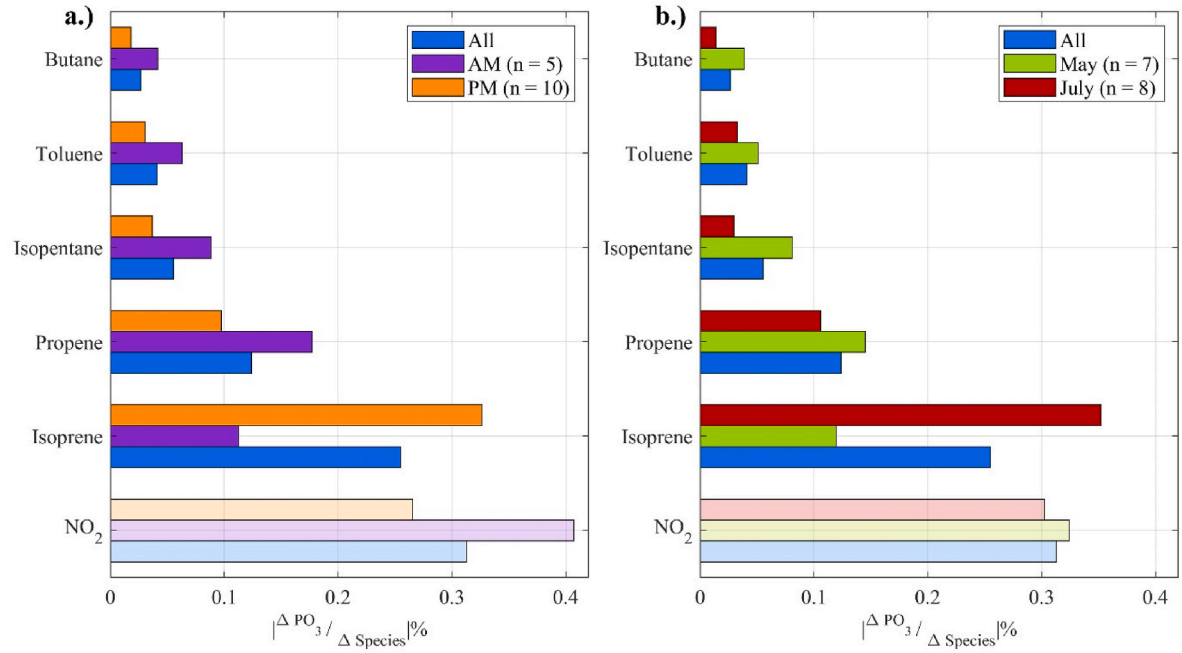

Fig. 5. Median modeled percent PO_3 change per percent species change for samples with VOC-limited PO_3 (based on Fig. 2). Top 5 species are ranked by overall sensitivity and includes **(a)** AM (purple), PM (orange), and all (blue) median sensitivity and **(b)** May (green), July (red), and all (blue) median sensitivity. NO_2 sensitivity is included for comparison (Based on Fig. 2) with a transparent color to indicate the inverse relationship with PO_3.

afternoon temperatures contribute to greater BVOC emissions (Coates et al., 2016). A 1% change in the isoprene concentration will have a bigger impact on PO_3 in the afternoon (0.33%) than in the morning (0.20%). Because isoprene is highly reactive, a small increase in isoprene at greater initial concentrations will have a compounding effect on ozone production through multi-generational chemistry. Every other VOC included in Fig. 5a has a greater impact in the morning than afternoon. Of these, the ones with the biggest diurnal variations, relative to their percent change in PO_3 are isopentane, toluene, and butane. There is a possible nighttime buildup of these anthropogenic VOCs, due to persistent emissions as well as a lower planetary boundary layer depth which contributes to greater morning VOC concentrations (Ring et al., 2023). In the morning, when PO_3 is greatest, PO_3 is most sensitive to anthropogenic VOCs.

The comparison between May and July demonstrates a similar pattern. Isoprene is the only VOC in this list to have a greater impact on PO_3 in July than May. The difference is a factor of three; a 1% change in isoprene causes a 0.12% change in PO_3 in May and a 0.37% change in July. The later summer is more sensitive to BVOC while May is more sensitive to anthropogenic VOC.Supplemental Text S2explores the sensitivity of PO_3 to HCHO, which is mainly a secondary product of VOC oxidation in the spring and summer and an important contributor to total OH reactivity and HO_2 production.

3.3. *Chemical mechanism comparison*

It is too computationally expensive to use explicit chemical mechanisms such as MCM in regulatory air quality models, instead condensed mechanisms such as CB6r2 are used. We repeat the previous model calculations using CB6r2 to highlight differences in model results owing to the use of this condensed chemical mechanism.

Calculated PO_3 is sensitive to the choice of chemical mechanism.

When using MCM, PO_3 is 20% higher on average compared to CB6r2 (Fig. 6a). This result is consistent across all simulations ($R^2 = 0.91$) and is invariant between spring and summer. Fig. 6b compares the two production terms of PO_3 (first two terms of Equation (5)) for CB6r2 versus MCM. Ozone production from CB6r2 is 14% slower than MCM for the reaction of HO_2 with NO and 28% slower for RO_2 + NO reactions, with both channels contributing roughly equally to total PO_3. Predicted NO is the same for both mechanisms (Fig. S8), thus differences are most likely related to radical concentrations and/or rate coefficients. Radical concentrations are 31% higher on average in MCM (Fig. 6c). Though the comparisons of HO_2 and RO_2 have slopes of 0.93 (Fig. 6c), there are consistent offsets between the two mechanisms as shown by a negative y-intercept ($y_{int} = -1$ ppt for HO_2 and $y_{int} = -4$ ppt for RO_2).

Differences in reaction rate coefficients may also contribute to differences in PO_3. The rate constant for HO_2 + NO is identical in both mechanisms ($3.45 \times 10^{-12} \times e^{(270/T)}$; Sander et al., 2011), therefore any differences in the rate of ozone production related to HO_2 and NO is strictly due to their concentrations. To compare the rate coefficients for RO_2 + NO between mechanisms, we calculate an effective rate constant that is weighted by all individual RO_2 reactions.

$$k_{eff} = \frac{\sum (k_i [NO][RO_2]_i)}{[NO] \sum [RO2]_i} \quad (7)$$

k_{eff} from CB6r2 is on average 96% of k_{eff} from MCM (Fig. 6d). This, along with greater total RO_2 concentrations, drives faster PO_3 in MCM. Variability of k_{eff} is slightly larger in CB6r2 than MCM (standard deviations are 0.39×10^{-12} and 0.24×10^{-12} cm^3/molecules/s, respectively) suggesting the weighted rate coefficients in the lumped mechanism are more sensitive to changes in VOC distributions than in the explicit MCM.

The samples with the biggest discrepancies in k_{eff} occur in the summer ($k_{eff,CB6r2}/k_{eff,MCM} = 94\%$), while the samples taken in May have better agreement ($k_{eff,CB6r2}/k_{eff,MCM} = 99\%$). One possible explanation for the seasonal difference in k_{eff} between the two mechanisms is the changing distribution of RO_2. In summer, a greater portion of RO_2 is BVOCs whereas in spring anthropogenic alkenes make up more of total RO_2. The effect of combining all isoprene products into a single species in CB6r2 will impact later-generation chemistry. This suggests that changing VOC distributions in urban areas may create spatial and/or seasonal bias in regional and global chemical transport models that use lumped schemes such as CB6r2. Higher k_{eff} in May is accompanied by lower total RO_2 concentrations, resulting in little seasonal difference in the agreement of PO_3 between MCM and CB6r2.

Fig. 7 shows median PO_3 curves generated using MCM (blue) and CB6r2 (green). As discussed previously, control PO_3 is on average 20% lower when using CB6r2 (black circles). However, the peak PO_3 when using CB6r2 is 41% lower than the median peak using MCM. Due to the condensed groups of peroxy radicals in CB6r2, there is less calculated OH reactivity and hence PO_3. The median value of LRO_x/LNO_x at the peak of the curves is consistent with the value using MCM (0.29 and 0.30

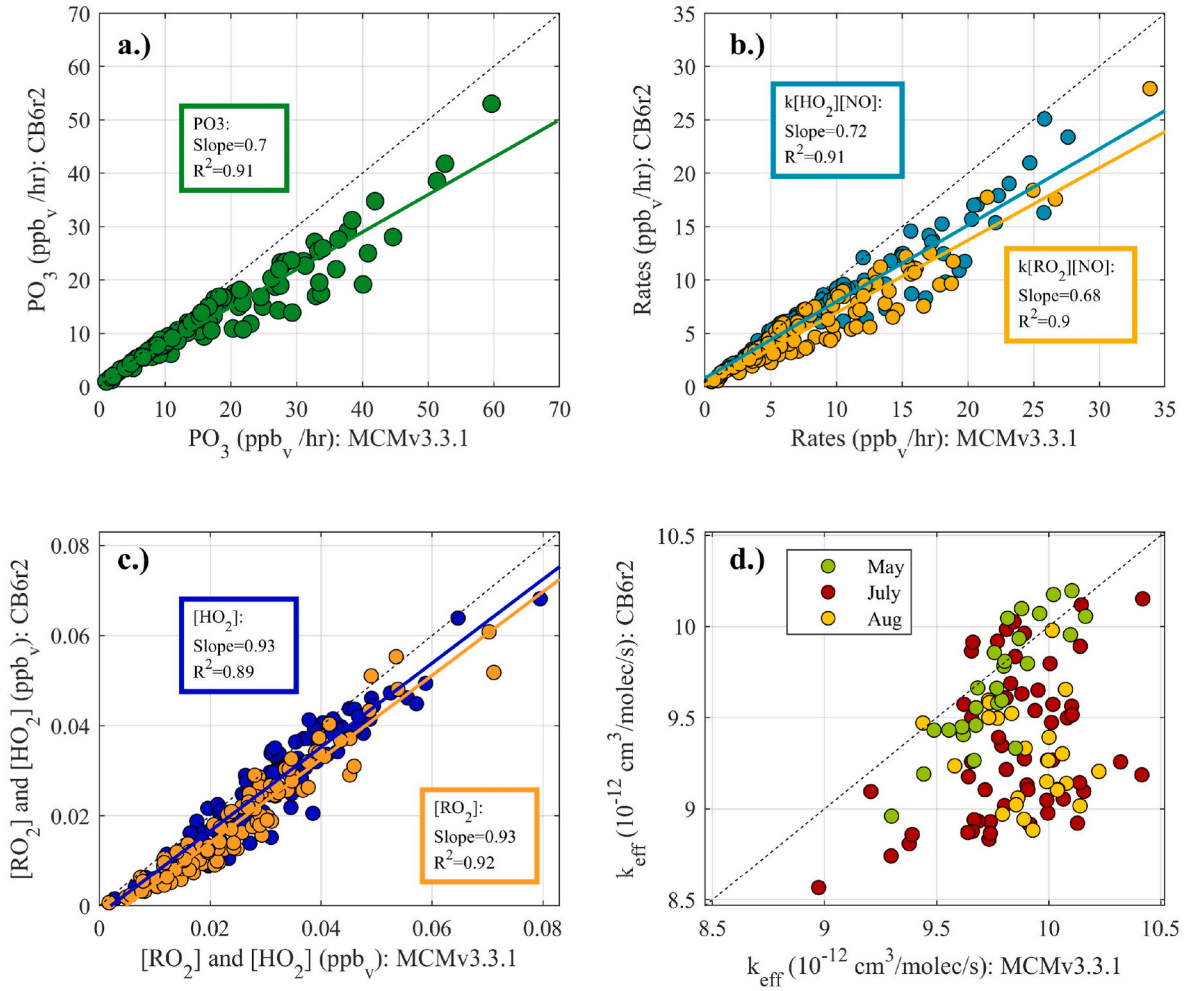

Fig. 6. A comparison of MCMv3.3.1 to CB6r2 output: **(a)** instantaneous netPO_3 (Equation (5)), **(b)** ozone production terms from HO_2 (blue) and RO_2 (yellow), **(c)** final mixing ratios of HO_2 (blue) and total RO_2 (yellow), **(d)** k- effective RO_2 + NO rate coefficient (Equation (7)) colored by the month of the observation. Lines of best fit are included in panels a-c. Dashed black lines are 1:1 reference lines.

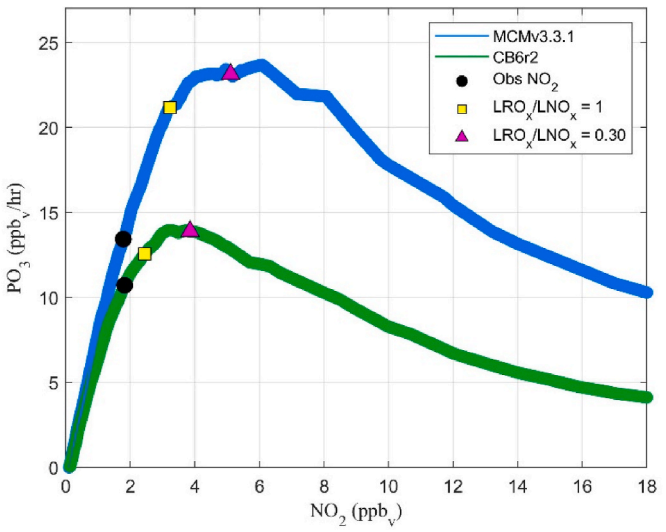

Fig. 7. Median PO_3 (ppb/hr) as a function of initial NO_2 concentration using MCMv3.3.1 (blue) and CB6r2 (green). Each line includes the observed NO_2 (black circle), LRO_x/LNO_x = 1 (yellow square), and LRO_x/LNO_x = 0.30 (pink triangle).

for CB6r2 and MCM, respectively). While the total concentrations of RO_2 vary between the mechanisms, the ratio of radical destruction from NO_x reactions to RO_2 self-reactions is the same. In Fig. 7 we use the value of 0.30 for the LRO_x/LNO_x threshold for both mechanisms (pink triangle).

Using the same transition thresholds ($0.3<=LRO_x/LNO_x<=1$), a greater portion of samples are in a VOC-limited regime (23%) or in transition (16%) using CB6r2. The peak of the CB6r2 ozone production curve occurs at lower NO_2 values, placing more samples at or beyond the peak of the curve and in the VOC-limited regime.

Fig. 8 compares the concentrations of specific RO_2 species between mechanisms. There are 13 subset groups in CB6r2 that react with NO (Hildebrandt Ruiz and Yarwood, 2013). The most abundant peroxy radical for both mechanisms is the methyl peroxy radical (CH_3O_2), which is represented explicitly as CH3O2 and MEO2 in MCM and CB6r2, respectively. On average, the calculated CH_3O_2 mixing ratio is slightly greater in MCM (7.9 ppt) compared to CB6r2 (7.1 ppt). In contrast, the mixing ratio of isoprene-derived RO_2 is slightly greater in CB6r2 (ISO2, 1.3 ppt) than the sum of seven isomers in MCM (ISOtotal, 1.1 ppt). The sum of the top five RO_2 in CB6r2 (14.5 ppt) is 23% greater than in MCM (11.8 ppt). However, the sum of the remaining RO_2, included as 'other' in Fig. 8, is 3.8 ppt (80%) greater in MCM. The greater total average RO_2 concentration using MCM shown in Fig. 8 is due to the accumulation of many minor RO_2 that are not explicitly represented in CB6r2.

Because OH reaction with VOC is the rate-liming step for RO_2 formation, OH reactivity (Equation (6)) is a useful metric for VOC contributions to RO_2 production. Fig. 9 shows speciated OHr from MCM and CB6r2 split into three groups: measured inorganics (green), measured organics (blue) and model-generated species (red) where each bar is an individual compound (or lumped group in the case of CB6r2). Modeled total OHr is 20% greater in MCM than CB6r2 (6.0 vs 5.0 s^{-1}). The contribution of measured inorganics is 6% lower in CB6r2 (MCM: 1.8 s^{-1}; CB6r2 1.7 s^{-1}), likely due to slight differences in rate coefficients. The contribution of measured organics is 13% lower in CB6r2 (MCM: 1.5

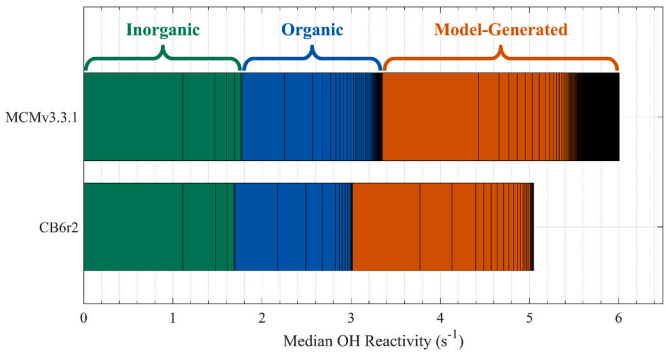

Fig. 9. The calculated median OH reactivity (Equation (6)) using MCMv3.3.1 and CB6r2. OH reactivity is separated by individual species and grouped by inorganic measured species (CO, NO_2, NO, SO_2, and O_3 in green), organic measured VOC (blue), and model-generated species (orange). MCMv3.3.1 has a total of 66 measured species and 2215 modeled species. CB6r2 includes 19 measured species and 32 modeled species.

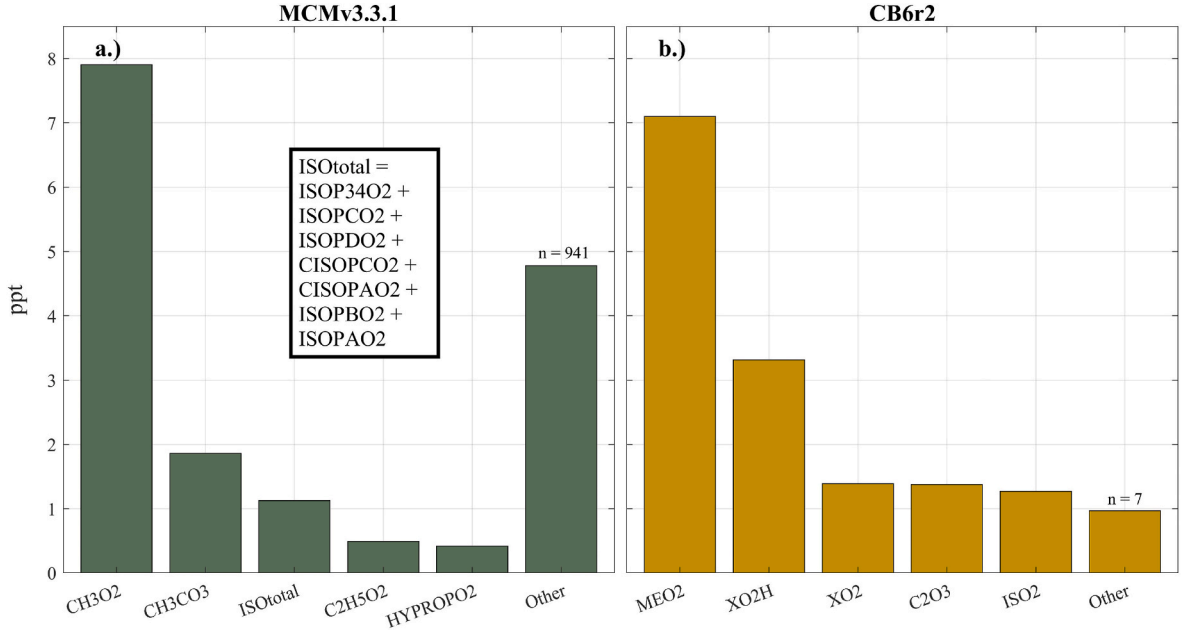

Fig. 8. The median concentrations of the 5 most abundant RO_2 and the summation of all other RO_2 species in **(a)** MCMv3.3.1 and **(b)** CB6r2. The seven isoprene products from OH addition given in Jenkin et al., (2015) are lumped together in MCM labeled as 'ISOtotal' for comparison with ISO2 in CB6r2.

s^{-1}; CB6r2: 1.3 s^{-1}) due to species grouping in the latter. Model-generated secondary VOC explains most of the difference in total OHr. The model-generated group accounts for 45% and 40% of total OHr for MCM and CB6r2, respectively. We calculate 2.7 s^{-1} from 2215 species in MCM and 2.0 s^{-1} from 32 lumped or explicit species in CB6r2, a difference of 26%. Results using both mechanisms exhibit similar rankings of the most reactive species in the model-generated species category. The largest model-generated contributors to OH reactivity include HCHO, acetaldehyde, first-generation isoprene oxidation products (methyl vinyl ketone and methacrolein), and glyoxal.

Of the MCM model-generated species, 99% have an OHr less than 0.01 s^{-1}, but together those species make up 20% of the overall model-generated OHr. Thus, secondary reaction products have a cumulatively significant impact on the total calculated ozone production. Measurements of speciated oxygenated VOC (oVOC), total OH reactivity and total RO_2/HO_2 concentrations would be valuable to validate these results in future studies.

4. Conclusions

We use aircraft observations from the LISTOS campaign to estimate PO_3 in the New York City area in the spring and summers of 2017–2019. We first classify the PO_3 regime by the response of PO_3 to initial NO_2 concentrations and find that 14% of air samples are in a VOC-limited regime. A transition between PO_3 regimes, defined as $0.3<=LRO_x/LNO_x<=1$, encompasses 16% of the data. In this range, PO_3 increases with increasing NO_x but is more sensitive (per molecule) to VOCs. Samples in a transition or in a VOC-limited regime are primarily located along the coast of Connecticut and in New York City. Using the LRO_x/LNO_x ratio to determine PO_3 regime indicates a higher portion of samples are VOC-limited as compared to only using the slope of the PO_3 isopleths to make this determination.

PO_3 exhibits diurnal and seasonal variations with maximum potential PO_3 being greater in the morning than the afternoon due to higher VOC concentrations in a shallower boundary layer. May is more likely to be VOC-limited (27% of samples) than July (14% of samples) or August (no samples), which is likely due to changes in total VOC availability rather than changing NO_x concentrations.

For samples within a VOC-limited regime, sensitivity tests reveal that isoprene concentrations have the greatest impact on PO_3, with a strong diurnal and seasonal variation. In the afternoon, PO_3 is most sensitive to isoprene, while in the morning, anthropogenic alkenes have a bigger effect on PO_3.

In the spring, focusing regulatory efforts on VOC reductions accompanied by NO_x reductions would most efficiently reduce PO_3 in this region. As temperatures warm, the ozone season is extending earlier into the spring (Ring et al., 2023). Therefore, ozone reduction strategies should be designed based on seasonal and diurnal differences in VOC concentrations and distributions.

We calculate PO_3 using CB6r2 for a more direct comparison to regulatory air quality models that use lumped schemes. We find that using CB6r2 reduces PO_3 and OH reactivity by 20% compared to results using MCMv3.3.1. These differences stem from assumptions regarding the photochemical kinetic parameters for the lumped RO_2 families. The value of LRO_x/LNO_x at the peak of these curves remains the same indicating the relative rates of radical destruction due to NO_x reactions and radical-self reactions are consistent between mechanisms. Using CB6r2, more samples are in a VOC-limited regime due to peak PO_3 occurring at lower values of NO_2.

The largest discrepancy in the OH reactivity comes from model-generated species, the most abundant of which include formaldehyde, acetaldehyde, first-generation isoprene oxidation products (methyl vinyl ketone and methacrolein), and glyoxal. Future observations of such oxidation products would provide important constraints in the calculation of PO_3 and improve confidence in our understanding of ozone production regimes. Volatile chemical products, which were not measured during LISTOS, are an increasingly important class of VOC and have been shown to increase modeled PO_3 by at least 10% (Coggon et al., 2021; Gkatzelis et al., 2021).

Our analysis of the VOCs observed during LISTOS shows spatial and temporal variations in PO_3 chemistry in densely populated areas. We emphasize that future aircraft field campaigns should measure a wide suite of VOCs, including HCHO, to provide a more detailed understanding of PO_3 chemistry. Implementing a more accurate representation of atmospheric chemical processes ensures the efficacy of regulatory models used to develop air quality policy.

CRediT authorship contribution statement

Abby E. Sebol: Conceptualization, Formal analysis, Investigation, Methodology, Visualization, Writing – original draft. **Timothy P. Canty:** Conceptualization, Funding acquisition, Methodology, Resources, Writing – review & editing. **Glenn M. Wolfe:** Funding acquisition, Methodology, Resources, Software, Writing – review & editing. **Reem Hannun:** Conceptualization, Methodology, Resources, Writing – review & editing. **Allison M. Ring:** Conceptualization, Methodology, Resources, Writing – review & editing. **Xinrong Ren:** Data curation, Investigation, Writing – review & editing.

Declaration of competing interest

The authors declare that they have no known competing financial interests or personal relationships that could have appeared to influence the work reported in this paper.

Data availability

Data will be made available on request.

Acknowledgements

We thank the National Science Foundation for support of the grant AGS-2023605, Maryland Department of the Environment (MDE) for support of the Regional Atmospheric Measurement Modeling and Prediction Program (RAMMPP; Grant #U00P3600274), the National Aeronautics and Space Administration (NASA) for support of the Atmospheric Composition Campaign Data Analysis and Modeling grant (ACCDAM; Grant # 80NSSC21K1448), and the North East States for Coordinated Air Use Management (NESCAUM; Grant # NESCAU-MUMDTSA20190603). All data used in this manuscript are publicly available from the NASA LISTOS archive website (https://www-air.larc.nasa.gov/cgi-bin/ArcView/listos?UMD-AIRCRAFT=1) last accessed January 2023. We thank Jason St. Clair for the CAFE data and Phil Stratton for assistance in data collection during the research flights. Finally, we thank Ross Salawitch, Russell Dickerson, and Akanksha Singh for their help in conceptualization, methodology, and visualization.

Appendix A. Supplementary data

Supplementary data to this article can be found online at https://doi.org/10.1016/j.atmosenv.2024.120417.

References

Anenberg, S.C., Horowitz, L.W., Tong, D.Q., West, J.J., 2010. An estimate of the global Burden of anthropogenic ozone and fine Particulate Matter on premature human Mortality using atmospheric modeling. Environmental Health Perspectives 118, 1189–1195.

Atkinson, R., Baulch, D.L., Cox, R.A., Crowley, J.N., Hampson, R.F., Hynes, R.G., Jenkin, M.E., Rossi, M.J., Troe, J., 2004. Evaluated kinetic and photochemical data for atmospheric chemistry: Volume I - gas phase reactions of O-x, HOx, NOx and SOx species. Atmos. Chem. Phys. 4, 1461–1738.

Atkinson, R., Baulch, D.L., Cox, R.A., Crowley, J.N., Hampson, R.F., Hynes, R.G., Jenkin, M.E., Rossi, M.J., Troe, J., 2006. Evaluated kinetic and photochemical data for atmospheric chemistry: Volume II - gas phase reactions of organic species. Atmos. Chem. Phys. 6, 3625–4055.

Baier, B.C., Brune, W.H., Lefer, B.L., Miller, D.O., Martins, D.K., 2015. Direct ozone production rate measurements and their use in assessing ozone source and receptor regions for Houston in 2013. Atmos. Environ. 114, 83–91.

Chen, S., Ren, X., Mao, J., Coauthors, 2010. A comparison of chemical mechanisms based on TRAMP-2006 field data. Atmos. Environ. 44, 4116–4125.

Chen, X., Millet, D.B., Singh, H.B., Coauthors, 2019. On the sources and sinks of atmospheric VOCs: an integrated analysis of recent aircraft campaigns over North America. Atmos. Chem. Phys. 19, 9097–9123.

Coates, J., Mar, K.A., Ojha, N., Butler, T.M., 2016. The influence of temperature on ozone production under varying NOx conditions – a modelling study. Atmos. Chem. Phys. 16, 11601–11615.

Coggon, M.M., Gkatzelis, G.I., McDonald, B.C., Coauthors, 2021. Volatile Chemical Product Emissions Enhance Ozone and Modulate Urban Chemistry, vol. 118. Proceedings of the National Academy of Sciences of the United States of America.

Couillard, M.H., Schwab, M.J., Schwab, J.J., Coauthors, 2021. Vertical profiles of ozone concentrations in the lower troposphere downwind of New York city during LISTOS 2018–2019. J. Geophys. Res. Atmos. 126.

Crawford, J., Davis, D., Olson, J., Coauthors, 1999. Assessment of upper tropospheric HOx sources over the tropical Pacific based on NASA GTE/PEM data: net effect on HOx and other photochemical parameters. J. Geophys. Res.-Atmos. 104, 16255–16273.

EPA: Summary Nonattainment Area Population Exposure Report. [Available online at: https://www3.epa.gov/airquality/greenbook/popexp.html.

Gery, M.W., Whitten, G.Z., Killus, J.P., Dodge, M.C., 1989. A photochemical kinetics mechanism for urban and regional scale computer modeling. J. Geophys. Res. Atmos. 94, 12925–12956.

Gkatzelis, G.I., Coggon, M.M., McDonald, B.C., Peischl, J., Aikin, K.C., Gilman, J.B., Trainer, M., Warneke, C., 2021. Identifying volatile chemical product tracer compounds in US cities. Environmental Science & Technology 55, 188–199.

He, H., Liang, X.Z., Sun, C., Tao, Z.N., Tong, D.Q., 2020. The long-term trend and production sensitivity change in the US ozone pollution from observations and model simulations. Atmos. Chem. Phys. 20, 3191–3208.

Hildebrandt Ruiz, L., Yarwood, G., 2013. Interactions between Organic Aerosol and NOy: Influence on Oxidant Production. University of Texas at Austin and ENVIRON International Corporation, 12-12.

Jenkin, M.E., Young, J.C., Rickard, A.R., 2015. The MCM v3.3.1 degradation scheme for isoprene. Atmos. Chem. Phys. 15, 11433–11459.

Kleinman, L.I., Daum, P.H., Lee, Y.N., Nunnermacker, L.J., Springston, S.R., Weinstein-Lloyd, J., Rudolph, J., 2001. Sensitivity of ozone production rate to ozone precursors. Geophys. Res. Lett. 28, 2903–2906.

Lindsay, A.J., Anderson, D.C., Wernis, R.A., Coauthors, 2022. Ground-based investigation of HOx and ozone chemistry in biomass burning plumes in rural Idaho. Atmos. Chem. Phys. 22, 4909–4928.

Loughner, C.P., Tzortziou, M., Follette-Cook, M., Coauthors, 2014. Impact of bay-breeze circulations on surface air quality and boundary layer export. J. Appl. Meteorol. Climatol. 53, 1697–1713.

Malley, C.S., Henze, D.K., Kuylenstierna, J.C.I., Vallack, H.W., Davila, Y., Anenberg, S.C., Turner, M.C., Ashmore, M.R., 2017. Updated Global Estimates of Respiratory Mortality in Adults >= 30 Years of Age Attributable to Long-Term Ozone Exposure, vol. 125. Environmental Health Perspectives.

Mao, J., Ren, X., Chen, S., Coauthors, 2010. Atmospheric oxidation capacity in the summer of Houston 2006: comparison with summer measurements in other metropolitan studies. Atmos. Environ. 44, 4107–4115.

Marvin, M.R., Wolfe, G.M., Salawitch, R.J., Coauthors, 2017. Impact of evolving isoprene mechanisms on simulated formaldehyde: an inter-comparison supported by in situ observations from SENEX. Atmos. Environ. 164, 325–336.

Mazzuca, G.M., Pickering, K.E., New, D.A., Dreessen, J., Dickerson, R.R., 2019. Impact of bay breeze and thunderstorm circulations on surface ozone at a site along the Chesapeake Bay 2011–2016. Atmos. Environ. 198, 351–365.

Mazzuca, G.M., Ren, X., Loughner, C.P., Estes, M., Crawford, J.H., Pickering, K.E., Weinheimer, A.J., Dickerson, R.R., 2016. Ozone production and its sensitivity to NOx and VOCs: results from the DISCOVER-AQ field experiment, Houston 2013. Atmos. Chem. Phys. 16, 14463–14474.

Mazzuca, G.M., Pickering, K.E., Clark, R.D., Loughner, C.P., Fried, A., Stein Zweers, D.C., Weinheimer, A.J., Dickerson, R.R., 2017. Use of tethersonde and aircraft profiles to study the impact of mesoscale and microscale meteorology on air quality. Atmos. Environ. 149, 55–69.

McDonald, B.C., de Gouw, J.A., Gilman, J.B., Coauthors, 2018. Volatile chemical products emerging as largest petrochemical source of urban organic emissions. Science 359, 760–764.

Oliveira, K., Guevara, M., Jorba, O., Querol, X., Garcia-Pando, C.P., 2023. A New NMVOC Speciated Inventory for a Reactivity-Based Approach to Support Ozone Control Strategies in Spain. Science of the Total Environment, p. 867.

Olson, J.R., Crawford, J.H., Davis, D.D., Coauthors, 2001. Seasonal differences in the photochemistry of the South Pacific: a comparison of observations and model results from PEM-Tropics A and B. J. Geophys. Res.-Atmos. 106, 32749–32766.

Olson, J.R., Crawford, J.H., Chen, G., Coauthors, 2004. Testing fast photochemical theory during TRACE-P based on measurements of OH, HO2, and CH2O. J. Geophys. Res.-Atmos. 109.

Ren, X.R., Salmon, O.E., Hansford, J.R., Coauthors, 2018. Methane emissions from the baltimore-Washington area based on airborne observation: comparison to emissions inventories. J. Geophys. Res.-Atmos. 123, 8869–8882.

Ring, A.M., Dickerson, R.R., Sebol, A.E., Ren, X., Benish, S.E., Salawitch, R.J., Galasyn, A., Miller, P.J., 2023. Anthropogenic VOCs in the long Island Sound, NY airshed and their role in ozone production. Atmos. Environ. 296, 119583.

Roberts, S.J., Salawitch, R.J., Wolfe, G.M., Marvin, M.R., Canty, T.P., Allen, D.J., Hall-Quinlan, D.L., Krask, D.J., Dickerson, R.R., 2022. Multidecadal Trends in Ozone Chemistry in the Baltimore-Washington Region. Atmospheric Environment, p. 285.

Sander, R., Baumgaertner, A., Gromov, S., Coauthors, 2011. The atmospheric chemistry box model CAABA/MECCA-3.0. Geosci. Model Dev. (GMD) 4, 373–380.

Schroeder, J.R., Crawford, J.H., Fried, A., Coauthors, 2017. New insights into the column CH2O/NO2 ratio as an indicator of near-surface ozone sensitivity. J. Geophys. Res.-Atmos. 122, 8885–8907.

Schroeder, J.R., Crawford, J.H., Fried, A., Coauthors, 2016. Formaldehyde column density measurements as a suitable pathway to estimate near-surface ozone tendencies from space. J. Geophys. Res.-Atmos. 121, 13088–13112.

Souri, A.H., Nowlan, C.R., Wolfe, G.M., Coauthors, 2020. Revisiting the Effectiveness of HCHO/NO2 Ratios for Inferring Ozone Sensitivity to its Precursors Using High Resolution Airborne Remote Sensing Observations in a High Ozone Episode during the KORUS-AQ Campaign, vol. 224. Atmospheric Environment.

St Clair, J.M., Swanson, A.K., Bailey, S.A., Hanisco, T.F., 2019. CAFE: a new, improved nonresonant laser-induced fluorescence instrument for airborne in situ measurement of formaldehyde. Atmos. Meas. Tech. 12, 4581–4590.

Strode, S.A., Ziemke, J.R., Oman, L.D., Lamsal, L.N., Olsen, M.A., Liu, J., 2019. Global changes in the diurnal cycle of surface ozone. Atmos. Environ. 199, 323–333.

Wolfe, G.M., Marvin, M.R., Roberts, S.J., Travis, K.R., Liao, J., 2016. The Framework for 0-D Atmospheric Modeling (F0AM) v3.1, vol. 9. Geoscientific Model Development, pp. 3309–3319.